Materials Today Bio 29 (2024) 101374

Contents lists available at ScienceDirect

Materials Today Bio

journal homepage: www.journals.elsevier.com/materials-today-bio

Sequential delivery of IL-10 and icariin using nanoparticle/hydrogel hybrid system for prompting bone defect repair

Xiaojun Li [a,1], Zeyue Sun [b,1], Xiushuai Shang [c,1], Liuting Chen [b], Xiaofeng Shi [a], Wei Xu [d], Shaotian Fu [a], Qingling He [b], Qihao Liang [a], Jie Ma [a], Xin Sun [e,**], Jiaju Lu [b,***], Wenjie Jin [a,*]

[a] *Shanghai Key Laboratory of Orthopaedic Implants, Department of Orthopaedic Surgery, Shanghai Ninth People's Hospital, Shanghai Jiao Tong University School of Medicine, No. 639 Zhizaoju Road, Shanghai, 200011, China*

[b] *School of Materials Science and Engineering, Zhejiang Sci-Tech University, Hangzhou, 310018, China*

[c] *Department of Orthopedics, The First Affiliated Hospital, Zhejiang University School of Medicine, No.79 Qingchun Road, Hangzhou, 310003, Zhejiang, China*

[d] *Department of Plastic and Reconstructive Surgery, Shanghai Ninth People's Hospital, Shanghai Jiao Tong University School of Medicine, No. 639 Zhizaoju Road, Shanghai, 200011, China*

[e] *Department of Orthopaedics, Shanghai Sixth People's Hospital Affiliated to Shanghai Jiao Tong University School of Medicine, No. 600 Yishan Road, Shanghai, 200233, China*

ARTICLE INFO

Keywords:
Injectable hydrogel
Nanoparticles
Sequential release
Immunomodulation
Osteogenesis

ABSTRACT

The treatment of large bone defects remains challenging due to the lack of spatiotemporal management of the immune microenvironment, inflammation response and bone remodeling. To address these issues, we designed and developed a nanoparticle/hydrogel hybrid system that can achieve the combined and sequential delivery of an anti-inflammatory factor (IL-10) and osteogenic drug (icariin, ICA). A photopolymerizable composite hydrogel was prepared by combining gelatin methacryloyl (GelMA) and heparin-based acrylated hyaluronic acid (HA) hydrogels containing IL-10, and poly(dl-lactide-co-glycolide) (PLGA)-HA nanoparticles loaded with ICA were incorporated into the composite hydrogels. The nanoparticle/hydrogel hybrid system demonstrates an array of features including mechanical strength, injectability and photo-crosslinking. The rapid release of IL-10 from the hydrogel effectively exerts immunomodulatory activity, whereas the long-term sustained release of icariin from the PLGA-HA nanoparticles significantly triggers the osteogenic differentiation of bone marrow-derived mesenchymal stem cells (BMSCs). Notably, the combined delivery of IL-10 and ICA from the hybrid system exhibit a synergistic effect for bone remodeling in a critical cranial defect rat model. Our findings indicate the importance of the immunomodulatory microenvironment and osteogenic differentiation for high-quality skull remodeling, and thus the dual-factor releasing nanoparticle/hydrogel hybrid system could be a promising candidate for repairing bone defects.

1. Introduction

Achieving ideal repair of bone defects caused by severe fracture, infection and tumor resection remains a substantial clinical challenge [1,2]. Patients with large bone defects require the implantation of a bone substitute to fill the missing location and restore normal structure and function [3]. Autologous and allogeneic bone grafts are currently the mainstay of bone defect treatment. However, their clinical use is hindered by several inherent limitations including the lack of donors, donor site morbidity, the difficulty to shape to match the defect contours, and risk of disease transmission [4]. To date, bone tissue engineering offers a promising approach for secondary reconstruction after bone defects [5]. Notably, the integration of various small molecule drugs and/or growth factors into different bioactive scaffolds has emerged as a boon for bone regeneration, which could achieve controlled release profiles and preserve their long-term activity [6].

Bone healing is a complex physiological process involving multiple biochemical cues in a time-sequential manner [7]. During the natural

* Corresponding author.
** Corresponding author.
*** Corresponding author.
E-mail addresses: doctor_sunxin@163.com (X. Sun), jiaju_lu@zstu.edu.cn (J. Lu), surgeonjin@126.com (W. Jin).
[1] These authors contributed equally to this work.

https://doi.org/10.1016/j.mtbio.2024.101374
Received 1 July 2024; Received in revised form 11 November 2024; Accepted 28 November 2024
Available online 3 December 2024

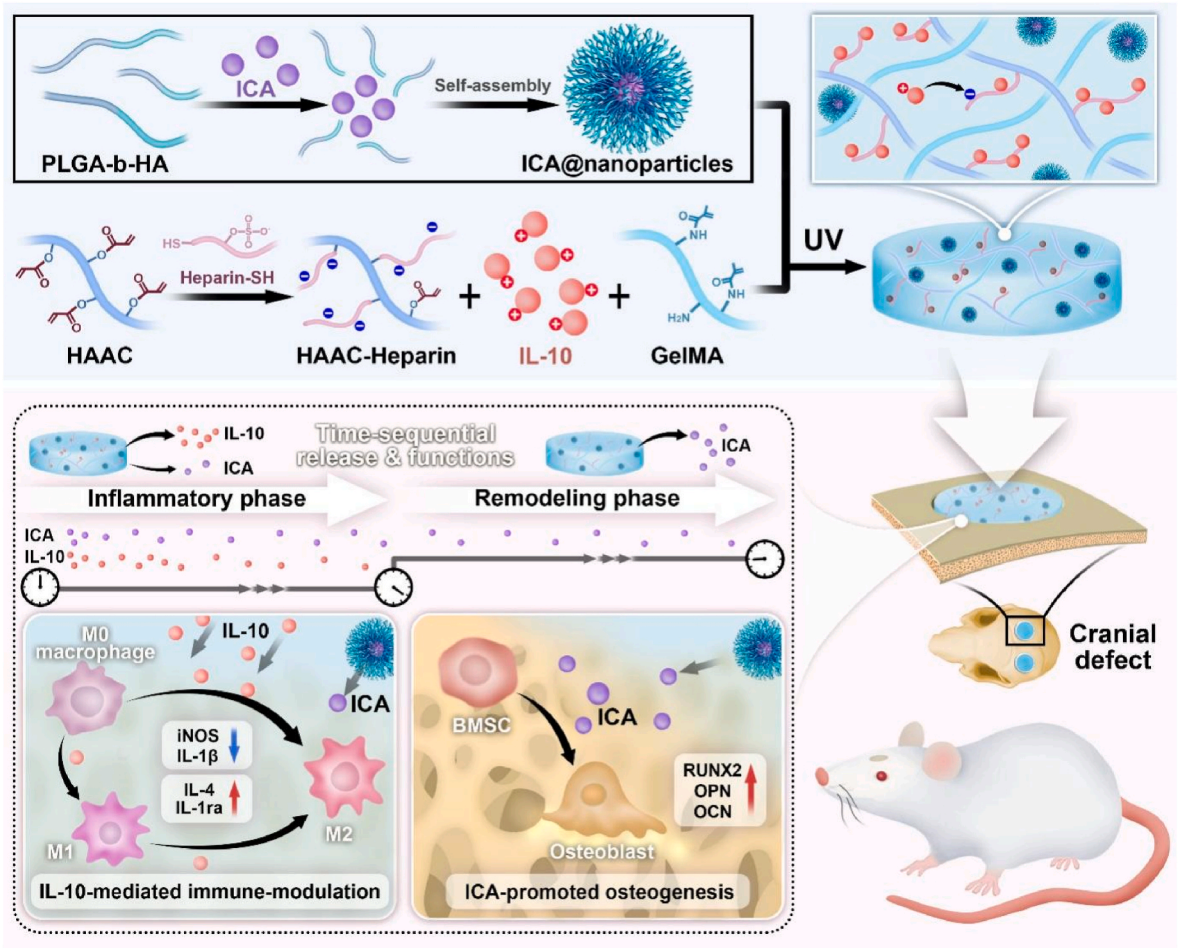

Scheme 1. Schematic diagram of the preparation of a multi-functional composite hydrogel with time-sequential IL-10 and ICA release and its immune-modulation and bone regeneration property.

process of bone repairing, resident and recruited macrophages at the site of injury initially polarize to pro-inflammatory M1 phenotype, producing pro-inflammatory cytokines [8]. M2 anti-inflammatory phenotype is enhanced during next phase, which produce anti-inflammatory factors that exert pro-tissue repair effects [9]. Several studies have proved that the altered polarization state of macrophages from M1 to M2 is crucial for facilitating the bone repair [10,11]. IL-10 is a potent anti-inflammatory factor with multiple biological functions, often used to induce M2 polarization of macrophages, thereby creating a favorable osteoimmune environment for bone regeneration [12,13]. However, the therapeutic efficacy of application of IL-10 is largely limited by short half-life, low local concentrations, and potential side effects [14]. It remains challenging to use biocompatible carriers to release IL-10 stably at localized injury sites to achieve its immunomodulatory effects for bone repair.

Various bio-scaffolds have been widely investigated for the delivery of therapeutic proteins [15]. Among them, hyaluronic acid (HA)-based hydrogels are potential candidates, as they are the major constituent of the natural extracellular matrix with good biological activity [16]. HA is also easily modified to expand its application, due to many reactive groups such as carboxyl, hydroxyl, and acetylamino in the molecular structure of HA [17]. For example, modification of HA hydrogel with heparin, a hypersulfated variant of heparan lacking domain structure, enables the capture of susceptible proteins and growth factors via by electrostatic action, allowing them to long-term release in a sustained manner *in vivo* and *in vitro* cultures [18]. Additionally, with appropriate crosslinking strategies such as photocrosslinking, HA hydrogel can be injected into irregularly shaped defect sites, providing unique advantages in bone repair [19].

Recent findings indicate that the coordinated crosstalk between macrophages and osteoblasts plays a key role in successful bone repair [20]. Therefore, promoting osteoblastic differentiation of bone marrow-derived mesenchymal stem cells (BMSCs) and inhibiting the inflammatory phenotype may have a synergistic effect in stimulating new bone formation. Icariin (ICA) is the main active ingredient extracted from *Epimedium*, a traditional Chinese medicine, known to possess a variety of pharmacological activities, including antioxidant, anti-tumor and neuroprotective activities [21–23]. Importantly, ICA can also significantly promote the osteogenic differentiation of human bone mesenchymal stem cells (hBMSCs) [24]. ICA has been incorporated into various biomaterial scaffolds to continuously release at bone defect sites to promote bone regeneration [25]. However, due to the inherent hydrophobicity of ICA, its loading homogeneity and quantity in hydrophilic hydrogels can be limited [20].

An interesting approach to reducing this challenge is to entrap pre-assembled drug delivery vehicle such as nanoparticle inside the hydrogel matrix, which are known as “plum pudding” hydrogels [26].This nanoparticle-hydrogel hybrid can improve the loading efficiency and controlled release of small molecule hydrophobic drug. However, previous studies have predominantly utilized inorganic or metallic materials as nanoparticles for bone regeneration, which generally exhibit moderate biocompatibility [27,28]. Amphiphilic block copolymer-based nanoparticles are considered effective carriers for solubilizing hydrophobic drugs with good biocompatibility, reducing the amount of drug required and minimizing unwanted side effects [29]. In view of all of the above, we synthesized self-assembling nanoparticles

composed of HA and poly(dl-lactide-co-glycolide) (PLGA), which could easily encapsulate hydrophobic drugs such as ICA. In addition, nanoparticle-hydrogel hybrid can provide appropriate controlled release rates of different drugs and factors, which has time-sequential drug release characteristics. Therefore, immune response and osteoblastic differentiation can be finely regulated via the different release sequence of drugs and factors, which is considered to be more closely related to the physiological bone healing process.

In the present study, we hypothesized that the sequential and combined delivery of IL-10 and ICA using a nanoparticle/hydrogel hybrid delivery system could synergistically induce bone regeneration. We designed and prepared a photopolymerizable HA/heparin-based hydrogel scaffolds by modifying HA chains with heparin and acrylate groups. To enhance the mechanical properties, degradation resistance, and stability time of heparin-based acrylated HA hydrogels (HAAC) *in vivo*, gelatin methacryloyl (GelMA) was added in appropriate proportions to create an injectable composite hydrogel scaffold. Heparin-modified HAAC/GelMA hydrogels (abbreviated as "gel") containing IL-10 were prepared, and PLGA-HA nanoparticles loaded with ICA were incorporated into the gels. The IL-10 released first had anti-inflammatory activities, which could induce more macrophages to convert to M2 phenotypes at an early stage. The subsequently sustained release of ICA from nanoparticles in the middle and late stages demonstrated a strong osteogenic effect. Through the above design of phased release, we have combined fast release and slow release to meet the needs of bone regeneration at each stage. The morphology, chemical and physical properties, and mechanical properties of the composite hydrogel were systematically investigated, as well as the sequential release behavior of IL-10 and ICA. The combined therapeutic efficacy of hybrid delivery system was evaluated using a rat cranial bone defect model (Scheme 1). Our findings have the potential to offer a new therapeutic approach for clinical management and provide new insights into the field of regenerative medicine.

2. Materials and methods

Synthesis and characterization of ICA-loaded PLGA-HA nanoparticles, HAAC, and Heparin-SH: The PLGA-HA block copolymers were synthesized as described in Huang et al. [30] Initially, a double bond was introduced on HA (Yuanye, China) to form acrylated hyaluronic acid (HAAC) via a thiol-ene click reaction. HAAC was synthesized in a two-step process: hyaluronic acid was first activated into HA-NHS, then reacted with NHS-Ac in a HEPES buffer, followed by dialysis and lyophilization to produce HAAC as a spongy solid. The degree of acrylation was measured using ^{1}H nuclear magnetic resonance (NMR) according to previous report [31]. Heparin (J&K, China) was modified by converting the carboxyl groups in its molecular structure into thiol groups via a carbodiimide reaction, yielding Heparin-SH. The percentage of conjugation of thiol groups on the Heparin-SH was determined by colorimetric Ellman's assay [32]. To obtain drug-loaded hydrogels, ICA and PLGA-HA were added to a centrifuge tube in a ratio of 338 mg: 10 mg: 1 mL of gel solution for self-assembly.

Preparation of the composite hydrogel: The concentrations of HAAC-Heparin and GelMA were determined according to previous reports [33,34]. Different ratios of HAAC (0.015 g), GelMA (0.025 g, EFL-GM-60, China), Heparin-SH (0.0015 g), and IL-10 (12 μL, Genscript, China), which constitute the 1 mL gel skeleton, were added to the LAP solvent. The mixture was magnetically stirred for 1 h in a water bath at 37 °C. The stirred hydrogel solution was then subjected to ultrasonic stirring to homogenously distribute the microspheres within the hydrogel solution. Finally, 0.1 % v/v LAP was added for 30 s under 405 nm wavelength illumination for photocrosslinking.

Transmission Electron Microscope (TEM): The size and morphology of the microspheres were observed using a transmission electron microscope (JEOL, Japan). The sample was treated with phosphotungstic acid negative staining solution, added dropwise on a copper grid, and dried by evaporation at room temperature. The microsphere particle size distribution was statistically analyzed using dynamic light scattering (Malvern, United Kingdom).

Scanning Electron Microscope (SEM): The dried composite hydrogel, loaded with or without nanoparticles, was fixed onto the stage using conductive adhesive. It was then sputter-coated with gold and observed using an SEM (Zeiss 500, Germany).

Mechanical test: Hydrogel samples were prepared into strips (10 cm × 1 cm x 0.2 cm), and their tensile properties were tested at 25 °C using a universal testing machine (Instron 5943, United States) at a rate of 20 mm/min for stress-strain testing.

Rheological analysis: Hydrogel samples were made into cylinders with a diameter of 20 mm and a height of approximately 6 mm. These were placed between 25 mm parallel plates with a spacing of 1000 μm. The storage modulus (G′) and loss modulus (G″) of the hydrogels were tested using a rheometer (Anton Paar MCR52, Austria) with a constant strain of 5 % and an angular frequency of 0.1–100 rad/s at 25 °C.

In vitro cytokine release assay: The hydrogel was placed in PBS buffer solution with pH = 7.2 and placed on a constant temperature shaker at 37 °C. At indicated time points, the released supernatant was collected and replaced with fresh PBS. The IL-10 concentrations were measured using a commercial ELISA kit (MultiSciences, China), following the manufacturer's instructions. The ICA concentrations were calculated by measuring the absorbance value of the solution at 268 nm by UV–Vis (Mapada P-7, China).

Isolation and culture of primary BMSCs: Two 1-week-old male Sprague-Dawley rats were euthanized and immersed in 75 % alcohol for 5 min, following established protocols [35]. Using sterilized forceps and scissors, the rat femur and tibia were separated, and muscle tissue was excised. The epiphyses of both bones were trimmed, and the marrow was thoroughly flushed out using α-MEM medium (Hyclone, USA) injected and withdrawn three times with a 1-mL syringe. The resultant single-cell suspension was centrifuged, the supernatant discarded, and the cell pellet resuspended in α-MEM medium supplemented with 10 % fetal bovine serum (Gibco, UK). The medium was replenished every 2–3 days until cells reached 80 % confluence, at which point they were passaged. Cells from passages 3–5 were used for subsequent experiments.

In vitro biocompatibility evaluation: After coculturing hydrogel and BMSCs or RAW 267.4 cells, Live-Dead staining was performed on day 1, and Cell Counting Kit-8 (CCK-8) assays were performed on day 1, 4, and 7 to assess cell viability. Briefly, after washing three times with PBS, the hydrogels were added with fluorescent dyes (KeyGEN, China) at 37 °C protect from light for 15 min. Then, the hydrogels were washed three times with PBS and observed using fluorescence microscopy (Olympus, Japan). For CCK-8 assay, the hydrogels were rinsed with PBS and incubated in 10 % CCK-8 reagent (Dojindo, Japan) containing medium for 2 h at 37 °C, and the absorbance was then determined at 450 nm using a spectrophotometer (Tecan, Switzerland).

Establishment of hydrogels/RAW264.7 cells/BMSCs co-culture system: To investigate the interaction between macrophages and osteoblasts, a co-culture system was established using a Transwell chamber. The hydrogel, containing 1×10^5 RAW264.7 macrophages, was placed in the upper compartment, while 1×10^6 BMSCs were positioned in the lower compartment. A polycarbonate membrane with a pore size of 1.0 μm separated the two compartments, allowing for the free exchange of cytokines and other soluble factors while maintaining physical separation between the cell types.

Immunofluorescence staining: Briefly, hydrogels were fixed with 4 % paraformaldehyde for 30 min at room temperature. After washing in PBS three times, samples were incubated for 10 min with 0.1 % Triton X-100. Hydrogels were then blocked with 5 % BSA for 30 min. After incubated with the primary antibodies at 4 °C overnight, the secondary antibodies were added in the dark for 1 h, followed by nuclei staining with DAPI at room temperature. Photographs were taken using a confocal laser scanning microscopy (Leica, Germany). Images were

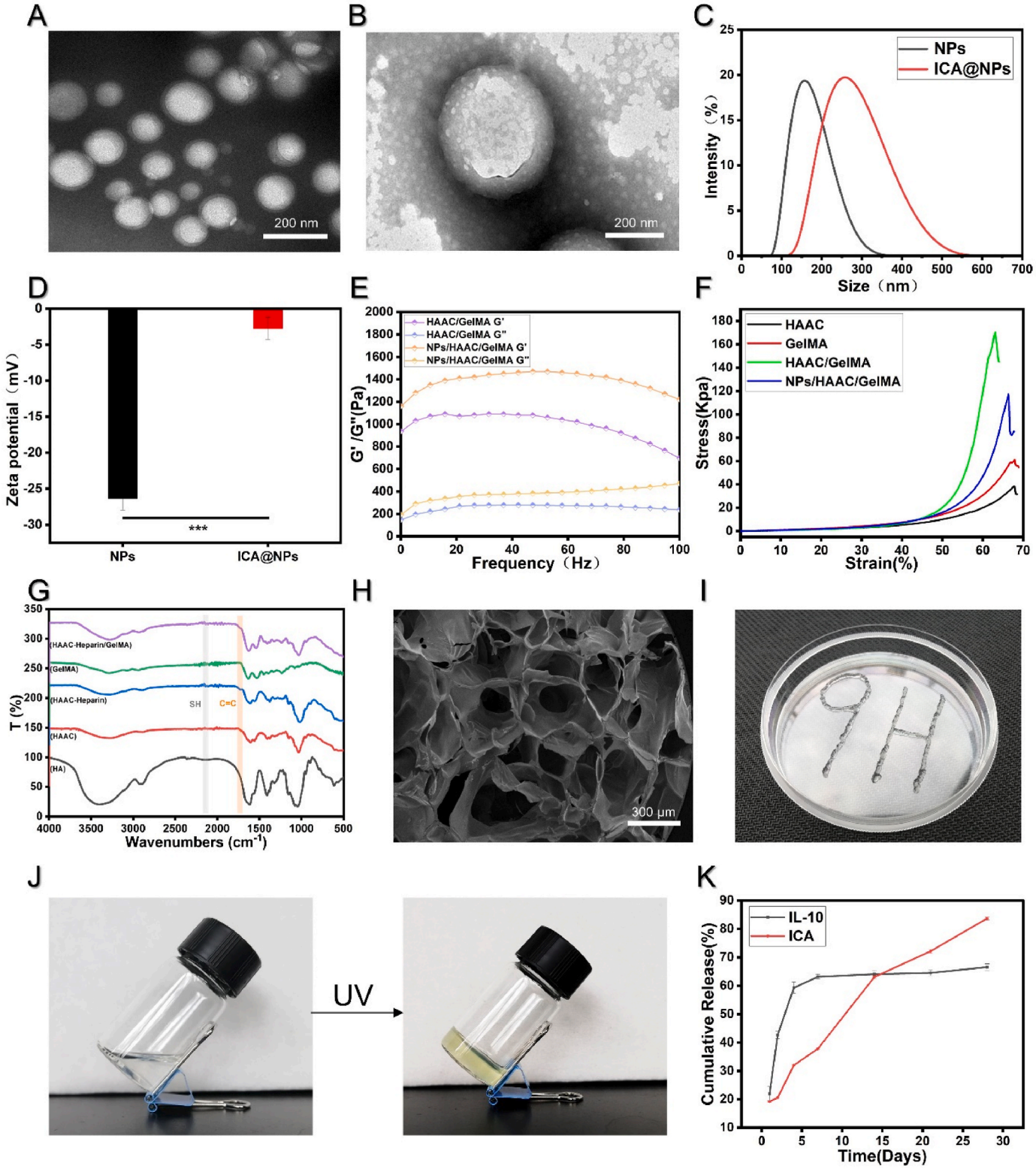

Fig. 1. Preparation and characterization of the nanoparticles and the hydrogel. A) TEM image of NPs. B) TEM image of ICA@NPs. C) Size distribution of NPs. D) Zeta potential of NPs and ICA@NPs (n = 3). E) Study of frequency-responsive rheological characteristics of the hydrogel under a 1 % strain condition. F) Compressive stress-strain curves. G) FTIR analysis of hydrogel. H) The SEM image of the hydrogel. I) Images reflecting the injectability and moldability of the hydrogel. J) Images showing the gelation process after UV. K) Cumulative release of IL-10 and ICA from the hydrogel. Data are shown as mean ± SD (***$p < 0.001$).

quantified by ImageJ software.

Quantitative Real-time Polymerase Chain Reaction (qRT-PCR) Analysis: A Universal RNA Purification Kit (EZBioscience, USA) was used to extract total RNA. The cDNA was synthesized using a Reverse Transcription Kit in a volume of 20 μl. qRT-PCR was performed using a SYBR Premix Ex TaqTM kit (TaKaRa, Japan) and an Applied Biosystems 7500 Real-Time PCR System (Applied Biosystems, USA). The sequences of the primers used are listed in Table S1.

Flow cytometry: The cells were blocked with 1 % bovine serum albumin (BSA) for 10 min. For surface marker detection, FITC-conjugated CD86 (BioLegend, China) was used for staining for 20 min at 4 4 °C overnight in the dark. For intracellular marker, cells were rinsed with perm/wash buffer (BioLegend, China) and then stained with APC-conjugated CD206 (BioLegend, China) for 20 min at 4 °C in the dark [36]. Stained cells were analyzed using a BD LSRFortessa flow cytometer (BD Biosciences, USA), and data were processed with FlowJo software.

Alkaline phosphatase (ALP) and Alizarin red S staining (ARS): For ALP staining, BMSCs were co-cultured with hydrogels after 7 days, and fixed in 4 % paraformaldehyde for 20 min. Then, they were stained using the BCIP/NBT alkaline phosphatase color development kit (Beyotime, China) according to manufacturer's protocol. For ARS staining, BMSCs were co-cultured with hydrogels after 21 days, and then fixed in 4 % paraformaldehyde for 20 min. They were stained using Alizarin Red S Staining Solution (Beyotime, China) according to the manufacturer's instructions. ImageJ software was used to quantitatively analyze the staining intensity of ALP and ARS.

Animals bone defect models: The critical-size skull defect rat model was used to evaluate the repair performance of the hydrogel [37]. After anesthesia, shaving and disinfection, a longitudinal incision was made along the cranial roof to separate skin, muscle and periosteum. The whole layer of bone tissue was removed with a dental implanter (W&H Implantedmed, Austria) and two full-thickness bone defects of 5 mm diameter on both side of the skull were created. Then, hydrogels were filled into the defects and the skin was sutured. The experimental groups were implanted with gel, IL-10@gel, ICA@gel and IL-10/ICA@gel and the control group was operated with nothing. All the experimental procedures and plans were carefully reviewed and approved by the Animal Ethical Committee of Shanghai Ninth People's Hospital with approval number SH9H-2024-A1013–1.

Microcomputed tomographic analysis (Micro-CT): Two months after surgery, the rats from the gel, IL-10@gel, ICA@gel and IL-10/ICA@gel and the control groups were sacrificed. Skulls were removed and fixed with 4 % paraformaldehyde for scanning. All samples were examined on a micro-CT scanning system (Bruker skyscan1176; Germany). After scanning, 3D images were reconstructed. The analyses of bone volume fraction (BV/TV) and bone mineral density (BMD) were then performed to estimate formations of new bones.

Histological assessment: The calvarial samples were fixed in 4 % paraformaldehyde for 24 h and decalcified in 20 % EDTA solution for at least 4 weeks. The samples were dehydrated in a graded series of ethanol (70–100 %) and embedded in paraffin [38]. Samples were then collected and stained with HE and Masson's trichrome and observed by light microscopy (Leica, Germany).

Immunohistochemistry staining: Briefly, tissue sections were deparaffinized and rehydrated in a graded series of ethanol. Endogenous peroxidase was then blocked using 3 % H_2O_2. After rinsing 3 times in PBS for 5 min, nonspecific binding was blocked in 5 % BSA for 30 min at room temperature. Then, the sections were incubated with the primary antibodies at 4 °C overnight, and the secondary antibodies were added in the dark for 1 h, followed by nuclei staining with DAPI at room temperature for 10 min. Immunoreactivity was visualized using a DAB chromogenic reagent (DAKO, Denmark). Immunohistochemical images were obtained by fluorescence microscopy, and digital images were recorded and evaluated using ImageJ software.

Statistical analysis: The data were expressed as the mean values ± standard deviation (SD). Statistical differences were assessed by Student's *t*-test (between two groups) and one-way analysis of variance (ANOVA) (among three or four groups) by using GraphPad Prism 9 software. Statistical significance was identified with p value less than 0.05 ($*p < 0.05$, $**p < 0.01$, $***p < 0.001$).

3. Results and discussion

3.1. Construction of ICA-loaded PLGA-HA nanoparticles

PLGA-HA is widely used as a matrix component for nanoparticles due to its good biocompatibility [30]. Herein, blank PLGA-HA (NPs) and ICA-loaded PLGA-HA nanoparticles (ICA@NPs) were constructed by a modified solvent-dialysis method. Transmission electron microscopy (TEM) images revealed that both blank and ICA-loaded NPs have a sphere-like morphology (Fig. 1A and **B**). Dynamic light scattering (DLS) measurements showed that blank NPs have a small size (~164 nm) with a narrow size distribution, whereas ICA@NPs have a larger hydrodynamic diameter of 255 nm (Fig. 1C). Additionally, a statistically significant reduction in surface charge was observed for ICA@NPs (−2.75 mV) compared to blank NPs (−26.37 mV) (Fig. 1D).

3.2. Characterization of the nanoparticle/hydrogel hybrid system

Numerous naturally derived biopolymers, such as gelatin and hyaluronic acid (HA), have been widely used in bone tissue engineering due to their good biocompatibility and degradability [39]. Both gelatin and HA can be easily functionalized because their molecular structures contain many active functional groups including carboxyl, hydroxyl, and amino groups. Recently, photocrosslinking has emerged as a promising strategy to create responsive hydrogels [40]. Gelatin methacryloyl (GelMA) has become a popular photocrosslinked hydrogel by modifying gelatin with methacrylic anhydride [41]. Similarly, photopolymerizable HA-based hydrogel scaffolds can be prepared by modifying HA chains with acrylate groups. In the present study, a composite hydrogel scaffold was prepared and crosslinked by combing GelMA and acrylated HA (HAAC) under an ultraviolet (UV) source. GelMA is a commercially available product with a amino substitution degree of 60 ± 5 %. NMR spectroscopy was conducted to quantify the grafting rate of HAAC (Fig. S1). The 1H NMR spectrum of HAAC showed new resonant peaks at 5.9 ppm and 6.3 ppm, representing the cis- and trans-acrylate hydrogens, respectively. The degree of acrylation was about 28.8 % by taking the ratio of new resonant peaks to the singlet peak at $\delta = 1.6$ (singlet peak of acetyl methyl protons in HA) [31]. A SEM image of the scaffold is shown in Fig. S2.

Hydrogels represent a kind of materials with a hydrophilic 3D polymer network that mimics the extracellular matrix of different tissues. However, they lack essential interaction between hydrophobic drugs and hydrogel matrix. To address this, we adopted the "plum pudding" strategy to form a nanoparticle/hydrogel hybrid system, which encapsulated drugs into nanoparticles and then loaded them into the composite hydrogels. The storage modulus (G′) and loss modulus (G″) of the composite hydrogels were measured with a plate-to-plate rheometer. As demonstrated by rheological results (Fig. 1E), the G′ and G″ of HAAC/GelMA and NPs/HAAC/GelMA composite hydrogel did not cross with the storage modulus dominant across the 0–100 Hz range, which exhibits classical hydrogel behavior. A significant increased G′ and G″ were observed in the nanoparticle/hydrogel hybrid system (NPs/HAAC/GelMA) compared to the HAAC/GelMA hydrogel (Fig. 1E, Fig. S3). In addition, according to the stress-strain curve of the uniaxial compression experiment, the composite hydrogel had a greater fracture strain than that of pure GelMA or HAAC, as shown in Fig. 1F and Fig. S4. The mechanical properties of the HAAC/GelMA composite scaffolds can be enhanced by the introduction of modified hyaluronic acid because the second HAAC flexible network provided support for the first GelMA rigid network. Incorporating NPs into hydrogels can increase the mechanical strength of composite hydrogels. In our study, the

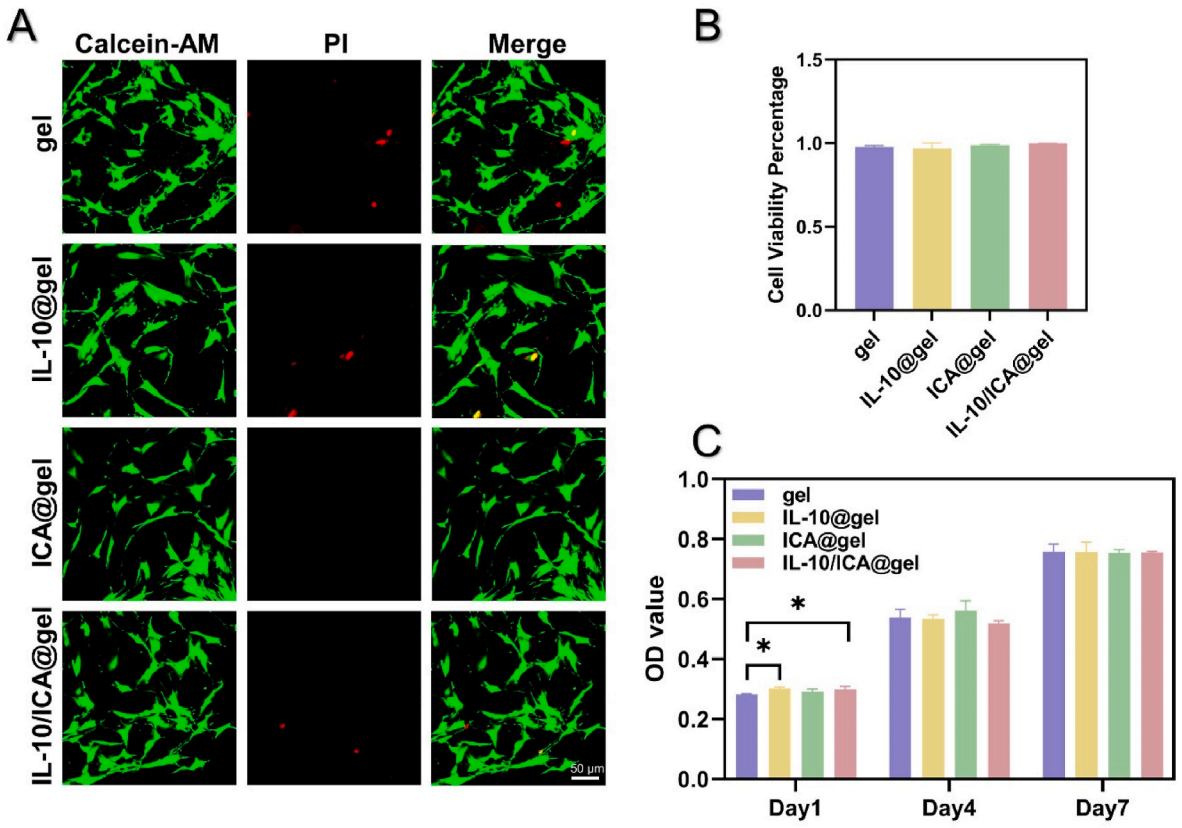

Fig. 2. Biocompatibility of the hydrogels *in vitro*. A) Live/dead assay of BMSCs cultured for 1 day of co-cultured on hydrogels. The green fluorescence indicates live cells stained by Calcein-AM. The red fluorescence indicates dead cells stained by PI. B) The quantitative data of live/dead assay. C) Cell proliferation of BMSCs for 1, 4 and 7 days of co-cultured on hydrogels were tested using CCK-8 analysis (n = 3) (*$p < 0.05$).

nanoparticle/hydrogel hybrid system (NPs/HAAC/GelMA) can tolerate higher stress and maintain the hydrogel state at high frequencies and strain than the HAAC/GelMA hydrogel, which makes favorable for bone healing.

After UV light exposure, the crosslinking density of HAAC/GelMA hydrogel increased, resulting in a higher compressive modulus (Fig. 1F). Furthermore, heparin-modified HA hydrogel was prepared via conjugation of heparin to HAAC, which enables the capture of IL-10 through electrostatic action, allowing for sustained long-term release of IL-10. By using cysteine as the standard, the amount of thiol groups in Hep-SH was 17.47 %. As shown in the FTIR spectra (Fig. 1G), a strong peak at 1645 cm^{-1} attributed to C=C double bonds in HAAC, and strong absorption at 2550-2590 cm^{-1} for HAAC-SH-Heparin attributed to the sulfhydryl group. SEM results revealed that the microstructural features of the NPs/HAAC/GelMA hydrogel, which exhibits a loose, networked structure with interconnected pores (Fig. 1H). The porous structure facilitates cell proliferation and tissue regeneration [42]. After loading ICA@NPs, the morphology of the hydrogel remains largely unchanged. Besides, the hydrogel can be injected and molded into various shapes to address diverse bone defects (Fig. 1I). As shown in Fig. 1J, the pregel solution exhibits excellent flowability before crosslinking, with gelation occurs after 30 s of UV irradiation in the presence of LAP.

In this study, we combined NPs, heparin-SH and hydrogels to construct a sequential release platform. HAAC-Heparin can provide rich negatively charged sites to bind the growth factor IL-10 through electrostatic interaction. In addition, PLGA-HA has an internal PLGA with hydrophobicity to bind ICA. The release behaviors of IL-10 and ICA were detected by ELISA kit and UV–Vis (Fig. 1K). Notably, 21.9 % of the loaded IL-10 was released from the hydrogel after one day. After 7 days, 63.1 % of the IL-10 was released, followed by the decrease release rate, which is conducive to the immunomodulation. Approximately 66.5 % of the loaded IL-10 was achieved by day 28. The limited release of IL-10 can be attributed to several factors, including: (1) Strong electrostatic interactions between IL-10 and heparin moieties of the HAAC-Heparin may lead to a slower diffusion rate. This can contribute to the observed release plateau, as some IL-10 may remain bound within the hydrogel. (2) The stability of IL-10 during the encapsulation and release processes is also a consideration. IL-10 has a certain half-life, and any degradation or conformational changes of IL-10 within the hydrogel may lead to incomplete release. The ICA release profile reveals that the additional sequestration by nanoparticles induces a slower and steadier release of ICA, allowing for long-term stimulation of osteogenic differentiation. A cumulative release of 83.7 % of ICA is observed by day 28. The combination of nanoparticles and hydrogels has successfully obtained the desired time-mediated sequential release process: IL-10 is rapidly released in the early phase, while ICA is gradually released over a prolonged duration.

3.3. *Biocompatibility of the hydrogel in vitro*

The biocompatibility of biomaterials is indispensable for their successful *in vivo* implantation [43]. HA and GelMA are both widely used in various biomedical applications due to their suitable biological properties and tunable physical characteristics [44,45]. The biocompatibility of the composite hydrogels was assessed using live/dead staining and cell counting kit-8 (CCK-8) assay. Specifically, BMSCs or RAW 264.7 were co-cultured with the different hydrogels for one day, followed by live/dead staining. As depicted in Fig. 2A–B and Fig. S5, all groups exhibited a substantial proportion of live cells (green fluorescence) and a negligible fraction of dead cells (red fluorescence), indicating that these hydrogels were non-cytotoxic. Next, the cells were co-cultured with the different hydrogels for 1, 4, and 7 days, followed by the CCK-8 assay.

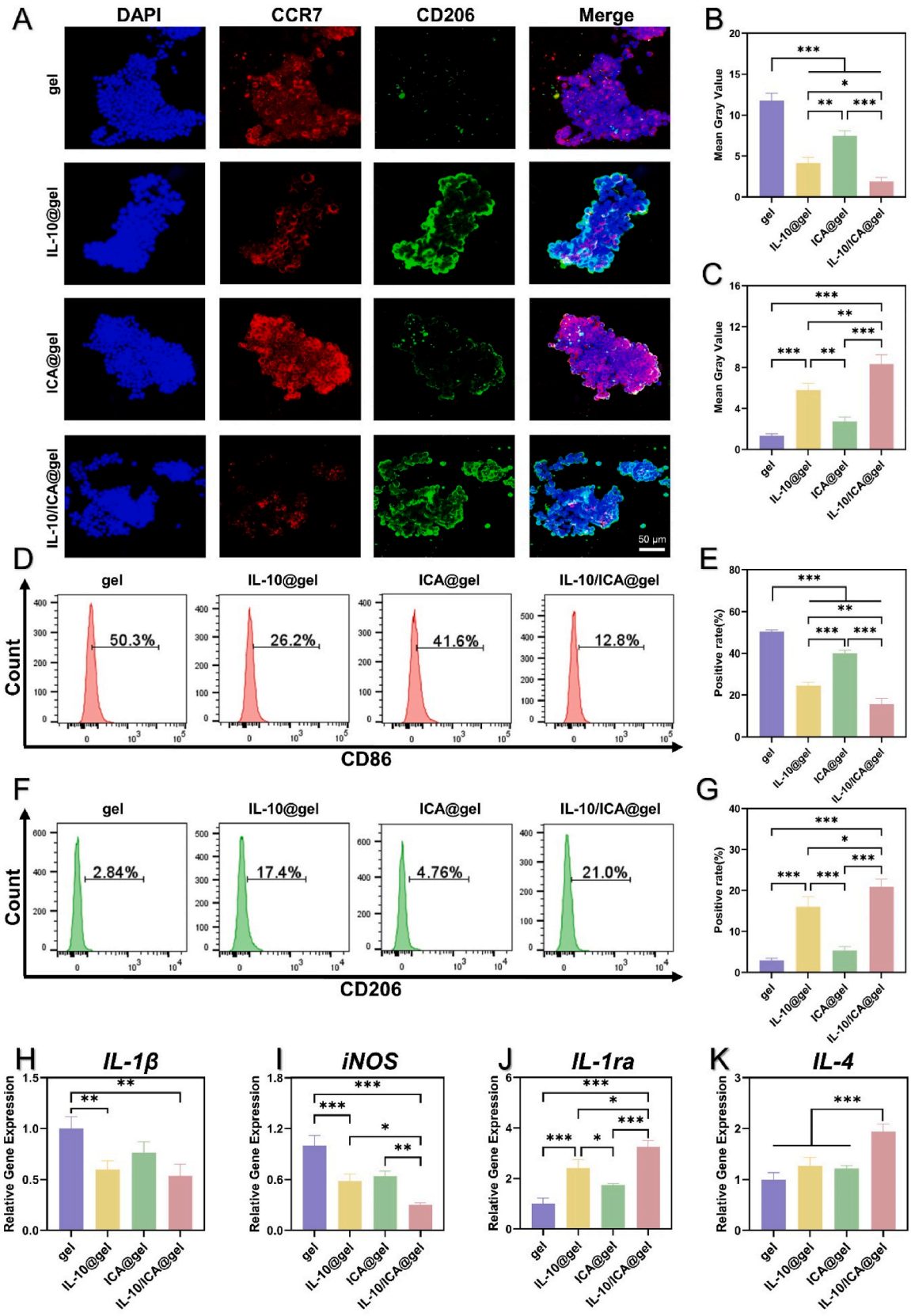

Fig. 3. Regulation of the macrophage-polarization phenotype *in vitro*. A) Representative CLSM images of surface markers CCR7 (red, M1 phenotype) and CD206 (green, M2 phenotype) expressions of RAW264.7 cells cultured with hydrogels for 3d by immunofluorescence analysis. B, C) Mean gray value of CCR7 and CD206 staining (n = 3); D, E) Flow cytometry analysis of CD86 (M1 phenotype) and CD206 expression of RAW264.7 cells cultured with hydrogels. F, G) The quantitative analysis of the percentage of M1 macrophages and M2 macrophages. H-K) Real-time PCR of M1 polarization-related IL-1β (H), iNOS (I) and M2 polarization-related IL-1ra (J) and IL-4 (K) (n = 3) (*$p < 0.05$, **$p < 0.01$, ***$p < 0.001$).

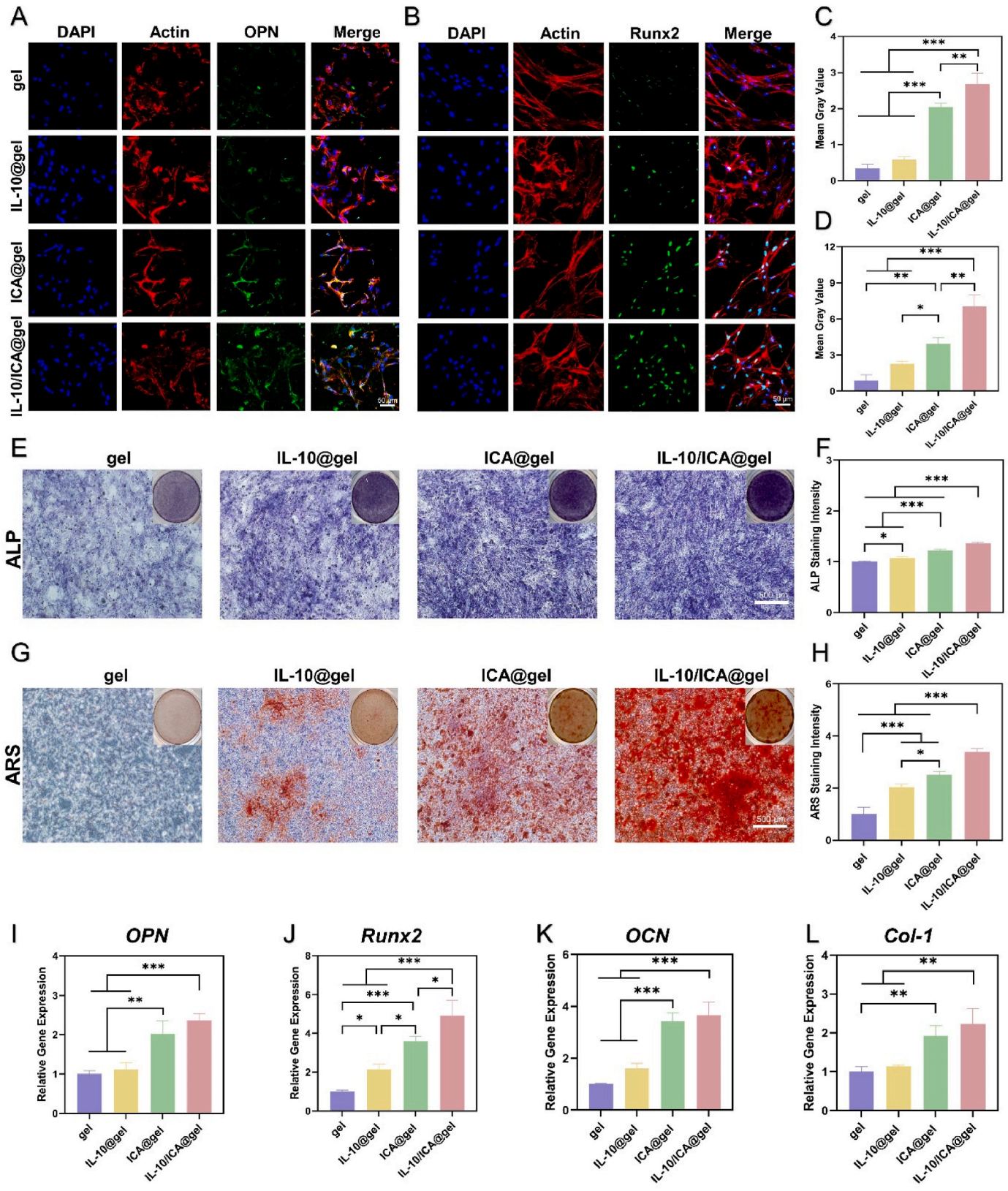

Fig. 4. Osteogenic differentiation of BMSCs stimulated by the hydrogel. A, B) Immunofluorescence staining images of OPN and Runx2 of BMSCs cultured with hydrogels for 7d. C, D) Quantification of the immunofluorescence density of OPN and Runx2 (n = 3). E, F) Alkaline phosphatase (ALP) of BMSCs cultured for 7d and quantitative evaluation of ALP staining intensity. G, H) Alkaline phosphatase S (ARS) staining of BMSCs cultured for 21 d and quantitative evaluation of ARS staining intensity. I-L) Relative mRNA expression of the osteogenic genes OPN, Runx2, OCN and Col-1 in BMSCs (n = 3) (*$p < 0.05$, **$p < 0.01$, ***$p < 0.001$).

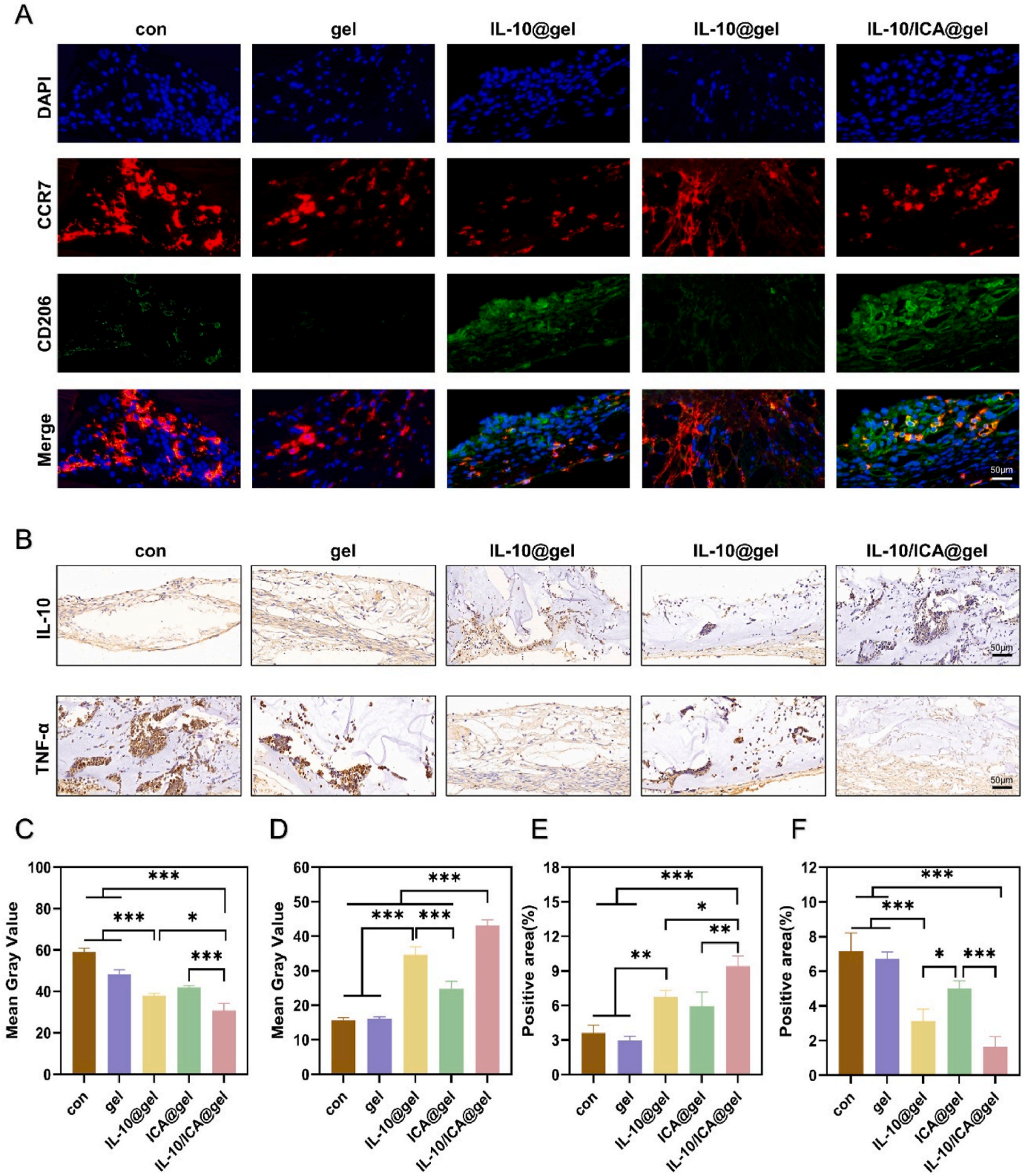

Fig. 5. *In vivo* immunomodulatory evaluations of the hydrogels. A) Representative images of surface markers CCR7 (red, M1 phenotype) and CD206 (green, M2 phenotype) expressions by immunofluorescence analysis; B) Immunohistochemistry of the IL-10 and TNF-α; C, D) The qualitative analysis of CCR7 and CD206; E, F) The qualitative analysis of IL-10 and TNF-α.(*$p < 0.05$, **$p < 0.01$, ***$p < 0.001$).

The results showed the hydrogels could promote cell proliferation of over time (Fig. 2C and Fig. S6). In addition, the cell adhesion was investigated by fluorescent staining of F-actin (by rhodamine-phalloidin, shown as red) and nuclei (by DAPI, shown as blue), respectively. As shown in Fig. S7, BMSCs adhered to the surface of the different hydrogels and spread well with polygonal structures after 1d and 3d of culture. Taken together, these results demonstrate that the composite hydrogels exhibited satisfactory biocompatibility.

3.4. Effect of the hydrogel regulation of the immune response

Bone tissue regeneration is hindered by the dysregulated, severe and persistent inflammation [46]. Regulating inflammation after injury is a promising approach to promote bone regeneration by not only preventing early-stage acute inflammation but also creating an immune microenvironment conducive to osteogenesis [47]. During the initial healing phase, immune cells rapidly infiltrate implanted materials and influence the local immune microenvironment [48]. As intrinsic immune cells, macrophages profoundly affect the endogenous repair process [49]. To study the ability of hydrogel to reprogram macrophages, lipopolysaccharides (LPS) were used to simulate the environment. Fig. 3A–C shows the immunofluorescence staining images and quantification of M1 marker (CCR7, red) and M2 marker (CD206, green) of RAW264.7 cells. M2 macrophages were significantly increased in the IL-10@gel and IL-10/ICA@gel groups compared to other groups. The results indicate that, with the inclusion of IL-10, the hydrogels exhibit an immunomodulatory effect characterized by M2 polarized RAW264.7 cells. Flow cytometry was used to further evaluate the macrophage phenotype switch at the cellular level (Fig. 3D–G). The CD86 positive cell ratio of the IL-10-loaded hydrogels was significantly lower than that of the IL-10-free hydrogels. Meanwhile, the CD206 positive cell ratio in the IL-10/ICA@gel group was significantly higher than that in the gel, IL-10@gel and ICA@gel groups. The results showed that the IL-10/ICA@gel significantly reduced CD86 expression and enhanced CD206 expression. Next, we detected a number of inflammatory factors. Additionally, the RT-qPCR results showed the significant down-regulation of pro-inflammatory cytokines, such as IL-1β and iNOS in the IL-10@gel and IL-10/ICA@gel groups (Fig. 3H and I). Meanwhile, the expression of anti-inflammatory cytokines (IL-4 and IL-1ra) was significantly up-regulated in IL-10@gel and IL-10/ICA@gel groups compared to the gel and ICA@gel groups (Fig. 3J and K). Thus, it seems that IL-10/ICA@gel could promote the secretion of anti-inflammatory cytokines and inhibit the expression of pro-inflammatory cytokines. It is worth mentioning that ICA have certain effects in macrophages M2 polarization [50]. In summary, the IL-10/ICA@gel could activate macrophage conversion to M2 phenotype, inhibit inflammatory responses and display robust immunomodulatory function.

3.5. In vitro performance of osteogenesis of the hydrogel

Immunofluorescence, alkaline phosphatase (ALP) staining, alizarin red S(ARS) staining, and gene expression levels of runt-related transcription factor 2 (Runx2), and osteopontin (OPN) related to osteogenesis were investigated to study the effects of the hydrogels on osteogenic differentiation. OPN and Runx2 are two important markers associated with osteogenic differentiation [51]. As shown in Fig. 4A–D, the expression of OPN and Runx2 in ICA-containing hydrogels (ICA@gel and IL-10/ICA@gel) was higher than in other groups. Interestingly, the OPN and Runx2 expression levels in IL-10@gel were higher than in the gel group, indicating that IL-10 can promote the expression of osteogenic markers. More importantly, the OPN and Runx2 expression levels in IL-10/ICA@gel were significantly higher than in ICA@gel, revealing that the combined release of IL-10 and ICA can synergistically promote the expression of OPN and Runx2. Fig. 4E–H shows the representative ALP staining, alizarin red S (ARS) staining and quantitative analysis. The IL-10/ICA@gel displayed the most intensified ALP staining compared with the other three groups, likely due to the presence of ICA. ARS staining showed a similar trend to ALP staining, indicating the best mineralization ability of IL-10/ICA@gel. In addition, the gene expression of OPN, Runx2, OCN and Col-1 were determined using RT-qPCR (Fig. 4I–L). Compared with other groups, the IL-10/ICA@gel significantly increased the expression of OCN and Runx2. Hydrogels containing ICA also exhibited significant upregulation of OCN and Col-1. These results indicate that IL-10/ICA@gel possesses a satisfactory ability to promote osteogenic differentiation due to the slow and long-term release of ICA. Moreover, the combination of IL-10 and ICA synergistically promoted osteogenic differentiation.

To further investigate the interaction between macrophages and osteoblasts, a sample/RAW264.7 cells/BMSCs co-culture system was established in a Transwell chamber. RAW264.7 cells were treated with different hydrogel groups and placed in the upper compartment, and BMSCs were placed in the lower compartment. After 7 or 21 days of co-cultivation, immunofluorescence staining, qPCR, ALP and ARS staining were used to evaluate the osteogenic differentiation of BMSCs. As shown in Figs. S8A–D, Immunofluorescence staining results showed that the fluorescence intensity of OPN was significantly higher in the IL-10/ICA@gel, ICA@gel, and IL-10@gel groups compared to the gel-only group. The ICA@gel group exhibited higher fluorescence intensity than the IL-10@gel group, with the highest intensity observed in the IL-10/ICA@gel group. For Runx2 expression, the fluorescence intensity was highest in the IL-10/ICA@gel group. ALP staining demonstrated that ALP activity was significantly higher in the IL-10/ICA@gel and ICA@gel groups compared to the IL-10@gel and gel-only groups (Figs. S8E–F). On day 21, Alizarin Red S (ARS) staining of calcium-binding proteins in the mineralized matrix revealed that the number and size of mineralized nodules in the IL-10/ICA@gel and ICA@gel groups were significantly larger than those in the other groups (Figs. S8G–H). The expression levels of genes related to osteogenesis, including OPN, Runx2, OCN, and Col-1, were also examined (Figs. S8I–L). These genes showed significantly higher expression in the IL-10/ICA@gel group compared to the other groups. These results indicate that the IL-10/ICA@gel formulation has a greater capacity for osteogenic differentiation compared to the other groups. Both macrophage-derived factors and ICA in the material delivery system play important roles in osteogenesis, and these components do not act in isolation but rather synergistically to enhance bone formation.

3.6. In vivo immunomodulation effect of the hydrogel

Bone defects rapidly mobilize immune cells from blood and surrounding tissues, activating a regeneration program. Manipulating the immune response to promote bone regeneration holds significant promise [52]. The immunomodulatory effect of the macrophage phenotype mainly manifested in the early stage [53]. As showed in Fig. 5**A**, C, and **D**, we performed immunofluorescence staining 7 days after implantation. The phenotypic transformation from M1 to M2 was mediated by labeling CCR7 (red) and CD206 (green). The IL-10/ICA@gel group exhibited larger areas and higher total fluorescence intensity of CD206 compared to other groups. Furthermore, hydrogels loaded with IL-10 showed a higher proportion of CD206 compared to those without IL-10. In contrast, the expression of CCR7 was significantly downregulated in the IL-10@gel and IL-10/ICA@gel, demonstrating that IL-10 released from the hydrogel could promote transformation of macrophage phenotype. To further validate the regulatory effect of the implanted hydrogels, immunohistochemical assays for representative proinflammatory cytokine TNF-α and anti-inflammatory cytokine IL-10 were performed to evaluate the inflammatory reaction (Fig. 5B, **E** and **F**). As expected, the control (con) and gel groups had the highest expression of TNF-α, suggesting a serious inflammatory response. In comparison to the con and gel groups, IL-10@gel and IL-10/ICA@gel groups upregulated IL-10 expression and downregulated TNF-α expression, which was particularly obvious in the IL-10/ICA@gel group. The results from both *in vitro* and *in vivo* suggested that the IL-10/ICA@gel effectively polarizes macrophages toward the M2 phenotype, and inhibiting inflammatory response, thereby creating a beneficial microenvironment for subsequent bone regeneration.

3.7. In vivo osteogenic capacity of the hydrogel

To verify the *in vivo* osteogenic ability of the composite hydrogel, we

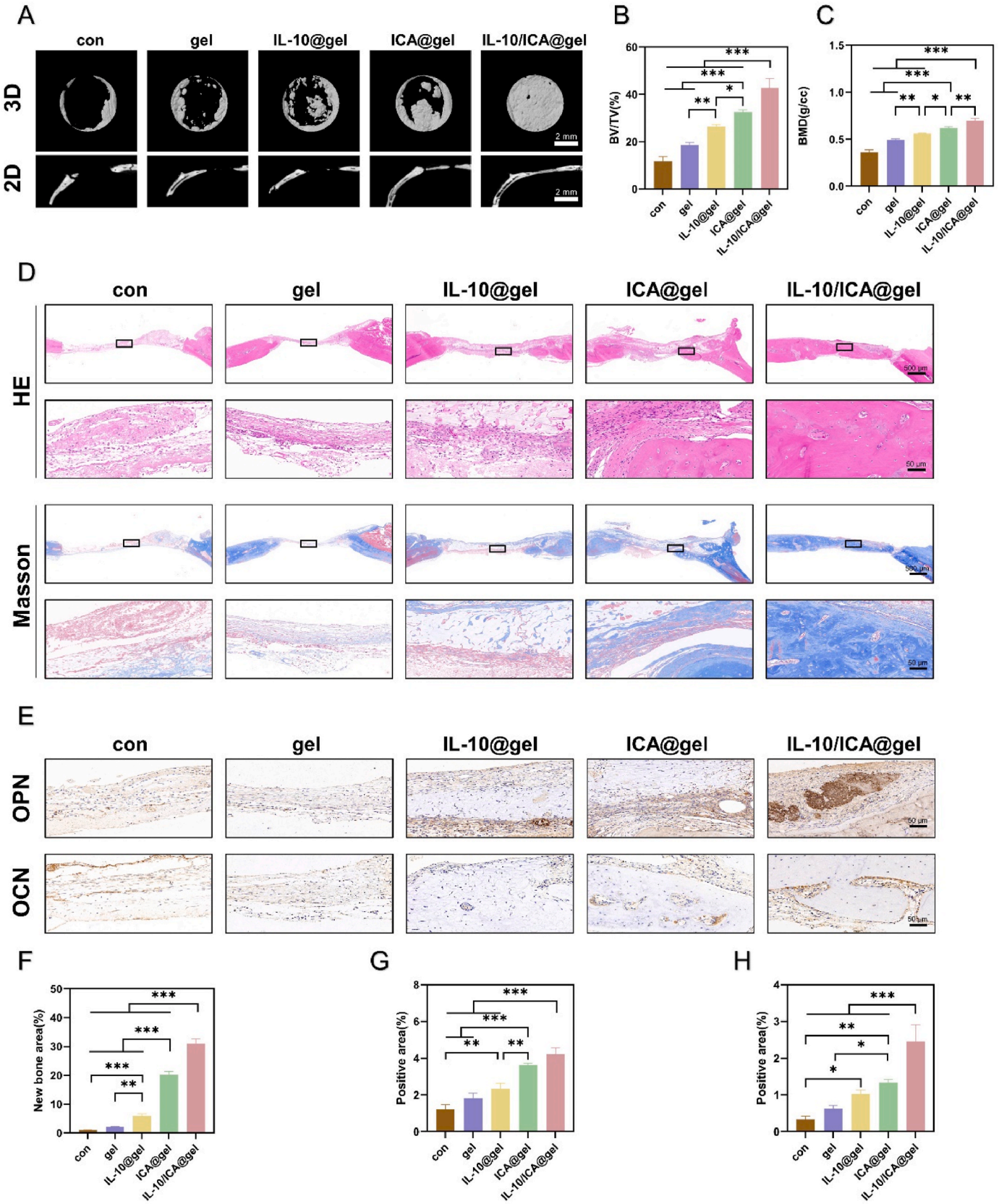

Fig. 6. *In vivo* osteogenesis capability of the hydrogel. A) Representative micro-CT images of skull defects implanted with the hydrogels. B, C) Quantitative evaluation of the osteogenic parameters, BV represents the amount of new bone volume, TV represents the amount of the total defect volume and BMD represents the new bone density. D) Representative H&E and Masson staining images of regenerative bone tissue at 8 week after surgery. E) Representative IHC staining of osteogenic marker (OPN and OCN); F) Quantitative analysis of new bone area; G, H) Quantitative analysis of OPN and OCN positive area. (*$p < 0.05$, **$p < 0.01$, ***$p < 0.001$).

created critical-sized cranial bone defects in SD rats. The hydrogels were injected to the defect sites. After 8 weeks, the samples were collected and analyzed. As depicted in Fig. 6A, micro-CT analysis revealed continuous new bone formation extending from the periphery to the defect center. The new bone formation of the IL-10/ICA@gel group was significantly large than the other groups, which indicated that the combination of IL-10 and ICA promoted the osteogenesis. In contrast, a few dense new bone tissues formed in the IL-10@gel and ICA@gel groups. The con and gel groups merely led to scattered bone regeneration. Specific parameters, including bone volume/tissue volume (BV/TV) and bone mineral density (BMD), were calculated (Fig. 6B and C). BV/TV represents the percentage of new bone tissue in the total defect volume, and BMD represents the bone density in the defect area. These key parameters revealed that the values of BV/TV and BMD were in the following order: IL-10/ICA@gel > ICA@gel > IL-10@gel > gel > con. More remarkably, the IL-10/ICA@gel show the highest values, which exhibits significant promotion effect on bone healing *in vivo*.

Subsequently, the microstructure of new bone formation in the defect sites were performed by H&E and Masson's trichrome staining. As shown in Fig. 6D, **F**, there were numerous new bone tissues observed in the IL-10/ICA@gel and ICA@gel groups. In particular, the defect areas of the IL-10/ICA@gel group were almost completely occupied by newly formed bone tissues. In contrast, the defect areas of the con and gel groups showed mainly fibrous tissue formation almost no new bone formation between host bones. These results indicated that IL-10 introduced with ICA can induce the more new bone regeneration. To further elucidate the osteogenic characteristics *in vivo*, the immunohistochemical staining of OPN and OCN was conducted. As displayed in Fig. 6E, G, H, the expression of these osteogenic markers in both IL-10/ICA@gel and ICA@gel groups was significantly higher than that in the con, gel and IL-10@gel groups. In particular, the IL-10/ICA@gel exhibited the most obvious positive regions, followed by those in ICA@gel, IL-10@gel and gel groups. Overall, the IL-10/ICA@gel demonstrated promising biomaterial potential due to the synergistic sequential effects of IL-10 and ICA, influencing M2 macrophage transition, reducing inflammation, and enhancing bone defect repair (Fig. S9).

4. Conclusions

In conclusion, we have developed a photopolymerizable nanoparticle/hydrogel hybrid system designed to modulate the immune microenvironment and promote osteogenic differentiation for treating bone defects. The combination of PLGA-HA nanoparticles and heparin-modified HAAC/GelMA composite hydrogels facilitated the sequential release of IL-10 and ICA. The rapid initial release of IL-10 changes the macrophage phenotype polarization from M1 to M2, improves osteoimmune microenvironment and the relatively slow and sustained delivery of ICA promotes osteogenic differentiation both in *vitro* and *in vivo*. Our findings illustrate that the coordinated delivery of IL-10 and ICA from this hybrid system synergistically enhances bone remodeling in a critical cranial defect rat model. Overall, this injectable immunomodulation-based hybrid system serves as an effective controlled drug delivery platform for the sequential release of multiple bioactive factors, offering a promising clinical strategy for treating bone defects.

CRediT authorship contribution statement

Xiaojun Li: Writing – original draft, Resources, Project administration, Methodology, Investigation, Formal analysis, Data curation, Conceptualization. **Zeyue Sun:** Writing – original draft, Resources, Methodology, Investigation, Formal analysis, Data curation. **Xiushuai Shang:** Supervision, Project administration. **Liuting Chen:** Resources, Methodology, Investigation, Formal analysis, Data curation. **Xiaofeng Shi:** Supervision, Resources, Methodology. **Wei Xu:** Resources. **Shaotian Fu:** Supervision. **Qingling He:** Resources, Methodology, Formal analysis, Data curation. **Qihao Liang:** Investigation. **Jie Ma:** Methodology. **Xin Sun:** Writing – review & editing, Visualization, Validation, Supervision, Resources, Project administration, Methodology, Funding acquisition. **Jiaju Lu:** Writing – review & editing, Validation, Supervision, Resources, Project administration, Funding acquisition, Conceptualization. **Wenjie Jin:** Writing – review & editing, Validation, Supervision, Funding acquisition.

Declaration of competing interest

The authors declare that they have no known competing financial interests or personal relationships that could have appeared to influence the work reported in this paper.

Acknowledgement

This work was supported by the National Natural Science Foundation of China (82071564, 82302676), Fundamental Research Funds for the Central Universities (24X010301321) and Fundamental Research Funds of Zhejiang Sci-Tech University (19212449-Y, 1112932612002).

Appendix A. Supplementary data

Supplementary data to this article can be found online at https://doi.org/10.1016/j.mtbio.2024.101374.

Data availability

Data will be made available on request.

References

[1] X. Shen, Y. Zhang, Y. Gu, Y. Xu, Y. Liu, B. Li, L. Chen, Sequential and sustained release of SDF-1 and BMP-2 from silk fibroin-nanohydroxyapatite scaffold for the enhancement of bone regeneration, Biomaterials 106 (2016) 205–216.
[2] J. Wang, Y. Wu, G. Li, F. Zhou, X. Wu, M. Wang, X. Liu, H. Tang, L. Bai, Z. Geng, P. Song, Z. Shi, X. Ren, J. Su, Engineering large-scale self-mineralizing bone organoids with bone matrix-inspired hydroxyapatite hybrid bioinks, Adv. Mater. (2024) e2309875.
[3] J. Zhou, C.W. See, S. Sreenivasamurthy, D. Zhu, Customized Additive Manufacturing in Bone Scaffolds-The Gateway to Precise Bone Defect Treatment, vol. 6, Research (Wash D C), 2023, p. 239.
[4] R. Dimitriou, E. Jones, D. McGonagle, P.V. Giannoudis, Bone regeneration: current concepts and future directions, BMC Med. 9 (2011) 66.
[5] S. Bose, N. Sarkar, Natural medicinal compounds in bone tissue engineering, Trends Biotechnol. 38 (4) (2020) 404–417.
[6] N. Yang, X. Yang, S. Cheng, X. Gao, S. Sun, X. Huang, J. Ge, Z. Han, C. Huang, Y. Wang, C. Cheng, L. Cheng, Magnesium implants with alternating magnetic field-enhanced hydrogen release and proton depletion for anti-infection treatment and tissue repair, Bioact. Mater. 38 (2024) 374–383.
[7] J. Long, Z. Yao, W. Zhang, B. Liu, K. Chen, L. Li, B. Teng, X.F. Du, C. Li, X.F. Yu, L. Qin, Y. Lai, Regulation of osteoimmune microenvironment and osteogenesis by 3D-printed PLAG/black phosphorus scaffolds for bone regeneration, Adv. Sci. 10 (28) (2023) e2302539.
[8] X. Dai, B.C. Heng, Y. Bai, F. You, X. Sun, Y. Li, Z. Tang, M. Xu, X. Zhang, X. Deng, Restoration of electrical microenvironment enhances bone regeneration under diabetic conditions by modulating macrophage polarization, Bioact. Mater. 6 (7) (2021) 2029–2038.
[9] Y.L. Yu, J.J. Wu, C.C. Lin, X. Qin, F.R. Tay, L. Miao, B.L. Tao, Y. Jiao, Elimination of methicillin-resistant Staphylococcus aureus biofilms on titanium implants via photothermally-triggered nitric oxide and immunotherapy for enhanced osseointegration, Mil Med Res 10 (1) (2023) 21.
[10] Y. Zhao, L. Bai, Y. Zhang, R. Yao, Y. Sun, R. Hang, X. Chen, H. Wang, X. Yao, Y. Xiao, R. Hang, Type I collagen decorated nanoporous network on titanium implant surface promotes osseointegration through mediating immunomodulation, angiogenesis, and osteogenesis, Biomaterials 288 (2022) 121684.
[11] S. Li, L. Zhang, C. Liu, J. Kim, K. Su, T. Chen, L. Zhao, X. Lu, H. Zhang, Y. Cui, X. Cui, F. Yuan, H. Pan, Spontaneous immunomodulation and regulation of angiogenesis and osteogenesis by Sr/Cu-borosilicate glass (BSG) bone cement to repair critical bone defects, Bioact. Mater. 23 (2023) 101–117.
[12] H. Shen, B. Xu, C. Yang, W. Xue, Z. You, X. Wu, D. Ma, D. Shao, K. Leong, J. Dai, A DAMP-scavenging, IL-10-releasing hydrogel promotes neural regeneration and motor function recovery after spinal cord injury, Biomaterials 280 (2022) 121279.
[13] O.R. Mahon, D.C. Browe, T. Gonzalez-Fernandez, P. Pitacco, I.T. Whelan, S. Von Euw, C. Hobbs, V. Nicolosi, K.T. Cunningham, K.H.G. Mills, D.J. Kelly, A. Dunne,

Nano-particle mediated M2 macrophage polarization enhances bone formation and MSC osteogenesis in an IL-10 dependent manner, Biomaterials 239 (2020) 119833.
[14] C. Wang, T. Li, X. Zeng, L. Wu, M. Gao, N. Tong, P. Duan, J. Liu, Sustained delivery of IL-10 by self-assembling peptide hydrogel to reprogram macrophages and promote diabetic alveolar bone defect healing, Dent. Mater. 39 (4) (2023) 418–429.
[15] F. Wang, H. Su, Z. Wang, C.F. Anderson, X. Sun, H. Wang, P. Laffont, J. Hanes, H. Cui, Supramolecular filament hydrogel as a universal immunomodulator carrier for immunotherapy combinations, ACS Nano 17 (11) (2023) 10651–10664.
[16] J. Li, H. Ke, X. Lei, J. Zhang, Z. Wen, Z. Xiao, H. Chen, J. Yao, X. Wang, Z. Wei, H. Zhang, W. Pan, Y. Shao, Y. Zhao, D. Xie, C. Zeng, Controlled-release hydrogel loaded with magnesium-based nanoflowers synergize immunomodulation and cartilage regeneration in tendon-bone healing, Bioact. Mater. 36 (2024) 62–82.
[17] C. Qi, Q. Sun, D. Xiao, M. Zhang, S. Gao, B. Guo, Y. Lin, Tetrahedral framework nucleic acids/hyaluronic acid-methacrylic anhydride hybrid hydrogel with antimicrobial and anti-inflammatory properties for infected wound healing, Int. J. Oral Sci. 16 (1) (2024) 30.
[18] G. Liu, R. Wu, B. Yang, Y. Shi, C. Deng, A. Atala, S. Mou, T. Criswell, Y. Zhang, A cocktail of growth factors released from a heparin hyaluronic-acid hydrogel promotes the myogenic potential of human urine-derived stem cells in vivo, Acta Biomater. 107 (2020) 50–64.
[19] K. Yu, H. Huangfu, Q. Qin, Y. Zhang, X. Gu, X. Liu, Y. Zhang, Y. Zhou, Application of bone marrow-derived macrophages combined with bone mesenchymal stem cells in dual-channel three-dimensional bioprinting scaffolds for early immune regulation and osteogenic induction in rat calvarial defects, ACS Appl. Mater. Interfaces 14 (41) (2022) 47052–47065.
[20] F. Zhang, M. Lv, S. Wang, M. Li, Y. Wang, C. Hu, W. Hu, X. Wang, X. Wang, Z. Liu, Z. Fan, J. Du, Y. Sun, Ultrasound-triggered biomimetic ultrashort peptide nanofiber hydrogels promote bone regeneration by modulating macrophage and the osteogenic immune microenvironment, Bioact. Mater. 31 (2024) 231–246.
[21] Z. Bi, W. Zhang, X. Yan, Anti-inflammatory and immunoregulatory effects of icariin and icaritin, Biomed. Pharmacother. 151 (2022) 113180.
[22] P. Kubatka, L. Koklesova, A. Mazurakova, A. Brockmueller, D. Büsselberg, M. Kello, M. Shakibaei, Cell plasticity modulation by flavonoids in resistant breast carcinoma targeting the nuclear factor kappa B signaling, Cancer Metastasis Rev. 43 (1) (2024) 87–113.
[23] L. Zheng, S. Wu, H. Jin, J. Wu, X. Wang, Y. Cao, Z. Zhou, Y. Jiang, L. Li, X. Yang, Q. Shen, S. Guo, Y. Shen, C. Li, L. Ji, Molecular mechanisms and therapeutic potential of icariin in the treatment of Alzheimer's disease, Phytomedicine 116 (2023) 154890.
[24] Y. Xu, Y. Jiang, B. Jia, Y. Wang, T. Li, Icariin stimulates osteogenesis and suppresses adipogenesis of human bone mesenchymal stem cells via miR-23a-mediated activation of the Wnt/β-catenin signaling pathway, Phytomedicine 85 (2021) 153485.
[25] L. Bai, Y. Liu, X. Zhang, P. Chen, R. Hang, Y. Xiao, J. Wang, C. Liu, Osteoporosis remission via an anti-inflammaging effect by icariin activated autophagy, Biomaterials 297 (2023) 122125.
[26] M.A. Campea, M.J. Majcher, A. Lofts, T. Hoare, A review of design and fabrication methods for nanoparticle network hydrogels for biomedical, Environ. Ind. Appl. 31 (33) (2021) 2102355.
[27] D.N. Heo, W.-K. Ko, M.S. Bae, J.B. Lee, D.-W. Lee, W. Byun, C.H. Lee, E.-C. Kim, B.-Y. Jung, I.K. Kwon, Enhanced bone regeneration with a gold nanoparticle–hydrogel complex, J. Mater. Chem. B 2 (11) (2014) 1584–1593.
[28] X. Li, Z. Yang, L. Fang, C. Ma, Y. Zhao, H. Liu, S. Che, A.V. Zvyagin, B. Yang, Q. Lin, Hydrogel composites with different dimensional nanoparticles for bone regeneration 42 (20) (2021) 2100362.
[29] D. Huang, P. Norat, L. Qi, A. Chernatynskaya, J.D. Cole, V.J. Mani, L. Xu, X. Liu, H. Yang, Consistent intraocular pressure reduction by solid drug nanoparticles in fixed combinations for glaucoma therapy, Adv. Sci. (2024) e2401648.
[30] J. Huang, H. Zhang, Y. Yu, Y. Chen, D. Wang, G. Zhang, G. Zhou, J. Liu, Z. Sun, D. Sun, Y. Lu, Y. Zhong, Biodegradable self-assembled nanoparticles of poly (D,L-lactide-co-glycolide)/hyaluronic acid block copolymers for target delivery of docetaxel to breast cancer, Biomaterials 35 (1) (2014) 550–566.
[31] W. Cao, J. Sui, M. Ma, Y. Xu, W. Lin, Y. Chen, Y. Man, Y. Sun, Y. Fan, X. Zhang, The preparation and biocompatible evaluation of injectable dual crosslinking hyaluronic acid hydrogels as cytoprotective agents, J. Mater. Chem. B 7 (28) (2019) 4413–4423.
[32] A.K. Jha, K.M. Tharp, J. Ye, J.L. Santiago-Ortiz, W.M. Jackson, A. Stahl, D. V. Schaffer, Y. Yeghiazarians, K.E.J.B. Healy, Enhanced Survival and Engraftment of Transplanted Stem Cells Using Growth Factor Sequestering Hydrogels, vol. 47, 2015, pp. 1–12.
[33] X. Zhu, X. Ding, Study on a 3D hydrogel-based culture model for characterizing growth of fibroblasts under viral infection and drug treatment, SLAS Discovery 22 (5) (2017) 626–634.
[34] R.N. Ghosh, J. Thomas, V.B. R, D.N. G, A. Janardanan, P.K. Namboothiri, M. Peter, An insight into synthesis, properties and applications of gelatin methacryloyl hydrogel for 3D bioprinting, Mater. Adv. 4 (22) (2023) 5496–5529.
[35] X. Sun, Z. Ma, X. Zhao, W. Jin, C. Zhang, J. Ma, L. Qiang, W. Wang, Q. Deng, H. Yang, J. Zhao, Q. Liang, X. Zhou, T. Li, J. Wang, Three-dimensional bioprinting of multicell-laden scaffolds containing bone morphogenic protein-4 for promoting M2 macrophage polarization and accelerating bone defect repair in diabetes mellitus, Bioact. Mater. 6 (3) (2021) 757–769.
[36] T. Wei, T. Pan, X. Peng, M. Zhang, R. Guo, Y. Guo, X. Mei, Y. Zhang, J. Qi, F. Dong, M. Han, F. Kong, L. Zou, D. Li, D. Zhi, W. Wu, D. Kong, S. Zhang, C. Zhang, Janus liposozyme for the modulation of redox and immune homeostasis in infected diabetic wounds, Nat. Nanotechnol. 19 (8) (2024) 1178–1189.
[37] X. Sun, J. Yang, J. Ma, T. Wang, X. Zhao, D. Zhu, W. Jin, K. Zhang, X. Sun, Y. Shen, N. Xie, F. Yang, X. Shang, S. Li, X. Zhou, C. He, D. Zhang, J. Wang, Three-dimensional bioprinted BMSCs-laden highly adhesive artificial periosteum containing gelatin-dopamine and graphene oxide nanosheets promoting bone defect repair, Biofabrication 15 (2) (2023).
[38] Z. Li, D. He, B. Guo, Z. Wang, H. Yu, Y. Wang, S. Jin, M. Yu, L. Zhu, L. Chen, C. Ding, X. Wu, T. Wu, S. Gong, J. Mao, Y. Zhou, D. Luo, Y. Liu, Self-promoted electroactive biomimetic mineralized scaffolds for bacteria-infected bone regeneration, Nat. Commun. 14 (1) (2023) 6963.
[39] W. Zheng, L. Ma, X. Luo, R. Xu, Z. Cao, Y. He, Y. Chang, Y. You, T. Chen, H. Liu, Ultrasound-triggered functional hydrogel promotes multistage bone regeneration, Biomaterials 311 (2024) 122650.
[40] Q. Zhang, K. Yan, X. Zheng, Q. Liu, Y. Han, Z. Liu, Research progress of photo-crosslink hydrogels in ophthalmology: a comprehensive review focus on the applications, Mater. Today Bio. 26 (2024) 101082.
[41] B. Lv, L. Lu, L. Hu, P. Cheng, Y. Hu, X. Xie, G. Dai, B. Mi, X. Liu, G. Liu, Recent advances in GelMA hydrogel transplantation for musculoskeletal disorders and related disease treatment, Theranostics 13 (6) (2023) 2015–2039.
[42] J. Chen, L. Yu, T. Gao, X. Dong, S. Li, Y. Liu, J. Yang, K. Xia, Y. Yu, Y. Li, S. Wang, Z. Fan, H. Deng, W. Guo, Nanofiber-induced hierarchically-porous magnesium phosphate bone cements accelerate bone regeneration by inhibiting Notch signaling, Bioact. Mater. 37 (2024) 459–476.
[43] J. Cao, G. He, X. Ning, X. Chen, L. Fan, M. Yang, Y. Yin, W. Cai, Preparation and properties of O-chitosan quaternary ammonium salt/polyvinyl alcohol/graphene oxide dual self-healing hydrogel, Carbohydr. Polym. 287 (2022) 119318.
[44] F. Shu, H. Huang, S. Xiao, Z. Xia, Y. Zheng, Netrin-1 co-cross-linked hydrogel accelerates diabetic wound healing in situ by modulating macrophage heterogeneity and promoting angiogenesis, Bioact. Mater. 39 (2024) 302–316.
[45] K. Yue, G. Trujillo-de Santiago, M.M. Alvarez, A. Tamayol, N. Annabi, A. Khademhosseini, Synthesis, properties, and biomedical applications of gelatin methacryloyl (GelMA) hydrogels, Biomaterials 73 (2015) 254–271.
[46] Y. Zhu, X. Yu, H. Liu, J. Li, M. Gholipourmalekabadi, K. Lin, C. Yuan, P. Wang, Strategies of functionalized GelMA-based bioinks for bone regeneration: recent advances and future perspectives, Bioact. Mater. 38 (2024) 346–373.
[47] M. Zhang, T. Yu, J. Li, H. Yan, L. Lyu, Y. Yu, G. Yang, T. Zhang, Y. Zhou, X. Wang, D. Liu, Matrix metalloproteinase-responsive hydrogel with on-demand release of phosphatidylserine promotes bone regeneration through immunomodulation, Adv. Sci. (2024) e2306924.
[48] S.J. Jiang, M.H. Wang, Z.Y. Wang, H.L. Gao, S.M. Chen, Y.H. Cong, L. Yang, S. M. Wen, D.D. Cheng, J.C. He, S.H. Yu, Radially porous nanocomposite scaffolds with enhanced capability for guiding bone regeneration in vivo, Adv. Funct. Mater. 32 (18) (2022).
[49] M. Sorkin, A.K. Huber, C. Hwang, W.F.t. Carson, R. Menon, J. Li, K. Vasquez, C. Pagani, N. Patel, S. Li, N.D. Visser, Y. Niknafs, S. Loder, M. Scola, D. Nycz, K. Gallagher, L.K. McCauley, J. Xu, A.W. James, S. Agarwal, S. Kunkel, Y. Mishina, B. Levi, Regulation of heterotopic ossification by monocytes in a mouse model of aberrant wound healing, Nat. Commun. 11 (1) (2020) 722.
[50] C. Zhang, Z. Cao, H. Lei, C. Chen, R. Du, Y. Song, C. Zhang, J. Zhou, Y. Lu, L. Huang, P. Shen, L. Zhang, Discovery of a novel small molecule with efficacy in protecting against inflammation in vitro and in vivo by enhancing macrophages activation, Biomed. Pharmacother. 165 (2023) 115273.
[51] X. Shao, Z. Hu, Y. Zhan, W. Ma, L. Quan, Y. Lin, MiR-26a-tetrahedral framework nucleic acids mediated osteogenesis of adipose-derived mesenchymal stem cells, Cell Prolif. 55 (7) (2022) e13272.
[52] W. Lin, Q. Li, L. Liu, Q. Wang, D. Zhang, F. Wang, R. Xu, Y. Fan, M. Xing, C. Zhou, Q. Yuan, Early infiltrating NKT lymphocytes attenuate bone regeneration through secretion of CXCL2, Sci. Adv. 10 (20) (2024) eadl6343.
[53] Y. Qiao, L. Yu, P. Yang, M. Chen, H. Sun, L. Wang, B. Wu, C.D. Oh, H. Yang, J. Bai, D. Geng, Spatiotemporal immunomodulation and biphasic osteo-vascular aligned electrospun membrane for diabetic periosteum regeneration, Adv. Sci. 10 (36) (2023) e2302874.